ORIGINAL RESEARCH ARTICLE

Silver-Decorated Reduced Graphene Oxide–Sulfonated Polyaniline Ternary Nanocomposite: A Highly Reliable Anti-Corrosion Coating Material for Mild Steel

Saurav Ramesh Nayak, Kikkeri Narasimha Shetty Mohana, Kamalon Rajitha, Ambale Murthy Madhusudhana, and Satishkumar R. Naik

The present work demonstrates the as-prepared silver (Ag)-decorated reduced graphene oxide (rGO) nanohybrid–sulfonated polyaniline (SPANI) as a highly efficient anti-corrosion coating material for mild steel (MS) corrosion. In this direction, graphene oxide (GO), rGO-Ag and rGO-Ag-SPANI were synthesized and characterized by Fourier transform infrared (FT-IR), x-ray diffraction (XRD), scanning electron microscopy (SEM), transmission electron microscopy (TEM), and Raman spectral studies. Different weight ratios of rGO-Ag and SPANI were dispersed in epoxy (EP) resin and coated on the MS surface by spin coating technique. The coated nanocomposites were examined by SEM, atomic force microscopy (AFM) and contact angle analyses. Electrochemical corrosion measurements of different compositions rGO-Ag and SPANI were carried out to analyze the influence of rGO-Ag-SPANI nanofiller in enhancing the anti-corrosion and barrier properties of EP resin. Results indicate that 1:2 composition of rGO-Ag and SPANI-dispersed epoxy coating (GASP-3) showed good corrosion protection against the corrosive electrolyte, and the value of $|Z|_{0.01 \text{ Hz}}$ was found to be in the order of $10^6 \ \Omega \ \text{cm}^2$. Further, the highest contact angle value of 93.4° in GASP-3 coating substantiates the electrochemical results. This could be ascribed due to the presence of more SPANI molecules in the coating matrix which effectively block the passage of corrosive electrolytes through the micropores of epoxy resin.

1. Introduction

Mild steel (MS) is one of the most used construction materials which has gained prominence in various fields. However, due to its low stability toward corrosion, it gets corroded easily in acidic, alkaline and saline environment due to chemical and/or electrochemical interaction between the metal and the corrosive media (Ref 1, 2). Low carbon alloy steels are employed in large metallic structures used in vessels, oil and gas industries, pipeline and docks, etc., over the marine environment (Ref 3). The destructive corrosive environment within these structures causes large economic loss and horrifying incidents. Hence, the development of new and potent corrosion-resistant coating materials is needed to enhance the durability of the metal and reduces economic and environmental losses. Several anti-corrosion techniques and methods have been developed to protect the metal from corrosion process (Ref 4). Polymer-based coatings is one of the most efficient approaches in this direction. The quality of the polymer coating can be further enhanced by adding a small amount of nanostructural materials as fillers which have large surface area and block the micropores of the coatings. An effective and improved anti-corrosion coating has been developed by the incorporation of metal oxide nanomaterials (Ref 5).

Carbon-based nanomaterials have attracted much attention due to its extraordinary mechanical, electrical, thermal and molecular barrier properties (Ref 6-8). In view of this, recently many researchers extensively used graphene oxide (GO) and modified graphene oxide (mGO) as nanofillers to effectively improve the corrosion resistance property of polymer-based coatings (Ref 9, 10). Further, in situ polymerization ensures uniform dispersion of GO which results in more close association between the polymer and the fillers through chemical bonding (Ref 11). Amrollahi et al. (Ref 12) polymerized aniline over GO by an in situ polymerization. GO–polyaniline (GO-PANI) incorporation showed an increase in weathering and corrosion resistance properties of epoxy coatings compared to that of GO-incorporated epoxy coating. Zhu et al. (Ref 13) employed an in situ polymerization technique to synthesize polypyrrole-functionalized graphene oxide (GO-PPy) for waterborne epoxy coatings by developing a polypyrrole (PPy) film on graphene oxide. The anti-corrosion and barrier ability of GO-PPy nanocomposites are associated with the passivation effect of PPy and impermeability offered by GO sheets.

Saurav Ramesh Nayak, Kikkeri Narasimha Shetty Mohana, Kamalon Rajitha, and Ambale Murthy Madhusudhana, Department of Studies in Chemistry, Manasagangothri, University of Mysore, Mysuru, Karnataka 570006, India; and Satishkumar R. Naik, Department of Studies in Chemistry, Karnatak University, Dharwad, Karnataka 580 003, India. Contact e-mail: drknmohana@gmail.com.

Javidparvar *et al.* (Ref 14) synthesized cerium-doped GO and incorporated in the epoxy matrix which was coated on the mild steel. They concluded that GO acts as a nanocontainer for the storage and release of cerium cations, which serves as an inhibiting species via ion exchange mechanism to provide a dual active/barrier corrosion resistance for epoxy coating. Ramezanzadeh *et al.* (Ref 15) incorporated the polyamidoamine (PMMA) dendrimer–GO sheets into the epoxy matrix to develop efficient anti-corrosive coating. They observed that the PMMA improves the dispersion of GO sheets in the epoxy by increasing the interlayer space of the GO nanosheets. Sari and Ramezanzadeh (Ref 16) non-covalently functionalized GO with hyperbranched polyamide to reinforce epoxy matrix to protect steel from corrosion. The functionalized GO sheets significantly enhanced the corrosion protection ability of the nanocomposite. In our recent studies, the addition of amine-functionalized GO into epoxy (EP) considerably enhanced the anti-corrosion performance and barrier property of the EP coating (Ref 17). It was proved that the decline in coating matrix from the metal in saline medium has been significantly reduced by the dispersion of FGO into EP. In another work, amine-functionalized GO using 8-bromo (Ref 1, 2, 4) triazolo [1,5,a] pyridine−2-amine was prepared and dispersed in polycaprolactone (PCL). The prepared FGO-PCL coating shows superior barrier and anti-corrosion performance (Ref 18).

Liao *et al.* (Ref 19) prepared the multi-functional sulfonated polystyrene/polyaniline/Ag (SPS/PANI/Ag) nanocomposite. The anti-corrosion studies showed that incorporation of SPS/PANI/Ag in waterborne alkyd resin considerably increases the anti-corrosion performance of alkyd resin. Zhou *et al.* (Ref 20) produced sulfonated polyaniline (SPANI)-anchored rGO and reported the enhanced corrosion inhibition and barrier performances of SPANI-rGO-incorporated EP coating. Qiu *et al.* (Ref 21) synthesized sulfonated PANI nanofiber and dispersed in epoxy to form a good composite coating over Q235 electrode. They observed that the composite coating with SPANI exhibited higher impedance modulus. Thus, review of literature indicated that SPANI in the epoxy matrix can enhance the anti-corrosive property.

In the literature, it has been reported that conductive polymers can limit the oxidation rate of metals and act as a corrosion protective system. PANI is one of the most investigated and popular types of conducting polymers, due to its facile synthesis, special chemistry (simple doping/de-doping chemistry) and environmental stability, whereas sulfonated polyaniline (SPANI) is a self-doped conducting polymer. SPANI can be used either as corrosion inhibitors through inclusion into the polymeric coatings or as protective coatings. The presence of many C=N repeating groups in SPANI structure makes it to be adsorbed on the metal surface. Polyaniline generates free electrons when the reduction process occurs, which promotes the formation of the passivation film on the steel surface (Ref 22, 23).

Epoxy coating is an isolated layer with holes to prevent the corrosive media permeating during the entire corrosion process; however, the nanofillers filled the holes effectively. As a conducting polymer/inorganic material, the nanofiller accepts the electrons released by metal dissolution. The accumulating iron ions (Fe^{2+} and Fe^{3+}) transform into the passive Fe_2O_3 and dense Fe_3O_4 as a protective film. Therefore, this occurrence allows much more time for the further proliferation of corrosive medium and water molecules to mild steel substrates.

Even though some researches have been focused on exploring the corrosion protection performances of the composites containing rGO with different polymers as a binary composite materials, very less work has been done with the ternary nanocomposites. Incorporation of metal nanoparticles into the conducting polymer is considered as an efficient way to improve the performance of the coating material (Ref 24, 25).

The present work demonstrates the as-prepared silver (Ag)-decorated reduced graphene oxide (rGO) nanohybrid–sulfonated polyaniline (SPANI) as a highly efficient anti-corrosion coating material for mild steel (MS) corrosion. Although the framework looks similar to that of Zhou et al., the synthesis of rGO with silver has an advantage over the previous work. Better electron transfer kinetics between the corrosive electrolyte and rGO-Ag-SPANI becomes important in prolonging the diffusion pathway and time. The nanosize of silver decorated on graphene oxide can block the porous structures; the induction of silver reduces the reactivity but ensures electron transfer, thereby acting as an additional passive barrier for the movement of electrolytes through the diffusion path. In the present work, we report the preparation of nanocomposites coatings which comprised SPANI and Ag-decorated rGO nanoparticles with an epoxy resin to improve the electrochemical performance and anti-corrosion behavior toward protection of the mild steel. Compared to the earlier work, our work showed better Icorr and Ecorr because of the better stability and durability of the coating material because of the presence of silver nanoparticles in the coating material.

2. Experimental

2.1 Materials and Instruments

Dimethyl sulfoxide (DMSO), trisodium citrate dihydrate, ammonium persulfate and aniline were purchased from Sigma-Aldrich. All other chemicals used were of analytical grade. Araldite epoxy resin and hardener were purchased from Huntsman Advanced Materials. The MS samples of dimension $5 \times 2 \times 0.3$ cm were used for corrosion studies. The chemical composition of the MS specimen is given in Table 1.

The synthesized GO and rGO-Ag/SPANI were characterized by XRD, SEM, TEM, FT-IR and Raman spectral studies. The FT-IR spectra were recorded using the Nicolet-5700 FT-IR spectrophotometer. The powder x-ray diffraction patterns were obtained using Rigaku miniflex II desktop x-ray diffractometer (Cu-Kα radiation, λ = 1.54 Å) at scan rate of 0.02° /s in 5−90° range. TEM analysis was done using Jeol/JEM 2100 having 200 kV voltage capacity. The Raman spectra were recorded with the HR800-UV confocal micro-Raman spectrometer Horiba Jobin Yvon, France, and the sample was excited with an inbuilt 532 nm wavelength laser. The contact angle measurements were performed using the KYOWA interface measurement with an analysis system of FAMAS.

Electrochemical impedance spectroscopy (EIS) and potentiodynamic polarization (PP) measurements were carried out using an electrochemical workstation (EIS, CHI608E, Austin, USA). A conventional three-electrode cell consists of |Ag/AgCl| as a reference electrode, platinum as a counter electrode and blank/coated MS sample as a working electrode with 1 cm^2 exposed area.

Table 1 Chemical composition of the mild steel specimen

Chemical	S	Mn	C	Si	P	Al	Fe
Wt.%	0.012%	0.13%	0.05%	0.05%	0.010%	0.1%	99.6%

2.2 Synthesis of rGO-Ag Binary Nanocomposite

The rGO-Ag nanohybrid was prepared by using DMSO as a reducing agent and trisodium citrate dihydrate as a capping agent to control the size of the nanoparticles. Briefly, 0.237 g of GO was dispersed in 50 ml DMSO. Simultaneously, 0.5 g of AgNO$_3$ was added to 50 ml of DMSO and stirred at 50 °C followed by addition of 0.8 g of trisodium citrate. Both the solutions were mixed and stirred for 6 h and filtered. The resulting precipitate was then washed thoroughly with distilled water and dried at 80 °C in vacuum for 48 h. The obtained rGO-Ag nanohybrid was then dried under infrared light.

2.3 Synthesis of Sulfonated Polyaniline (SPANI)

The aniline monomer (5 ml) was added into 20 ml of 1 M HCl solution and stirred for 15 min. To this solution, 5 g of ammonium persulfate (APS) dissolved previously in 1 M HCl solution (20 ml) was added dropwise at 5-6 °C with continuous stirring for 1 h and left overnight for polymerization. The resulting precipitated polyaniline (PANI) was collected by filtration and dried at 60 °C under vacuum for 24 h. Thus, obtained PANI (5 g) was then taken in a 500-ml RB flask. To this 20 ml of 1, 2-dichloroethane was added and heated to 60 °C under stirring for 4 h. 1 ml of chlorosulfonic acid diluted with 10 ml of 1,2-dichloroethane was added to this reaction mixture while stirring for 1 h. The resulting semisolid precipitate was separated by filtration, and it was then added to 300 ml of deionized water and stirred for 2 h at 50 °C to promote hydrolysis. The resulting solution was filtered through a cellulose membrane (0.22 μm pore size) under vacuum. Finally, the synthesized sulfonated polyaniline (SPANI) was dried in air at room temperature.

2.4 Synthesis of rGO-Ag-SPANI Ternary Nanocomposite

The binary nanocomposite of rGO-Ag (0.2 g) was dispersed in 50 ml of deionized water and sonicated in an ultrasonic bath for 30 min. In a 250-ml round-bottom flask, 20 ml of aqueous solution of SPANI was taken, and the above dispersion was added to it and stirred for 2 hrs at 60 °C then cooled and filtered. The sample thus collected was air-dried at 25 °C to obtain rGO-Ag-SPANI ternary nanocomposite. Three different compositions of rGO-Ag-SPANI nanocomposites were prepared by varying the weights of rGO-Ag and SPANI in the ratio of 1:0.5, 1:1 and 1:2 by the same method, and the resulting ternary nanocomposites were designated as rGO-Ag-SP-1, rGO-Ag-SP-2 and rGO-Ag-SP-3, respectively.

3. Results and Discussion

3.1 Fourier Transform Infrared Spectral Studies

The Fourier transform infrared (FT-IR) spectra of GO, rGO-Ag and rGO-Ag-SPANI are shown in Fig. 1. The broad band at
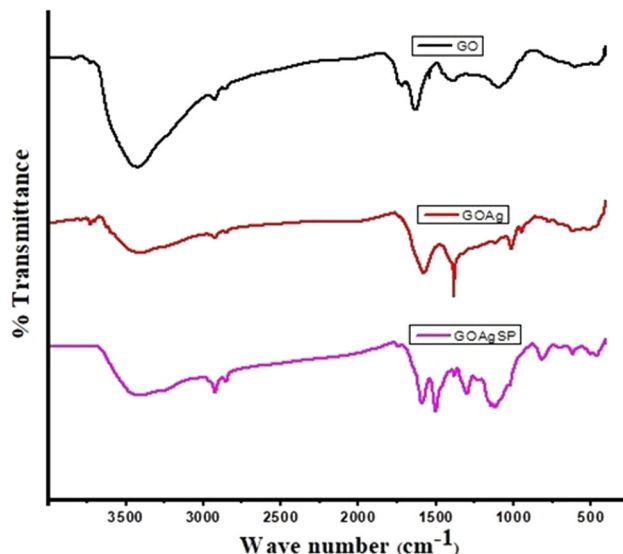
Fig. 1 FT-IR spectra of GO, rGO-Ag and rGO-Ag-SP

around 3433 cm^{-1} confirms the presence of -OH group in GO. The C-C and aromatic C=C stretching vibrations were noticed at 1393 cm^{-1} and 1631 cm^{-1}. The appearance of an intense band at 1722 cm^{-1} is attributed to C=O stretching vibration of carboxyl group. The band indicated at 1083 cm^{-1} is due to the epoxy (C-O- C) and 2923 cm^{-1} is because of = C-H groups. The significant reduction in the intensity of the absorption bands of the oxygen-containing functional groups in rGO-Ag can be probably due to the presence of Ag nanoparticles on the outer surface of GO and also because of the partial reduction of GO by DMSO during the synthetic process (Ref 26, 27). In rGO-Ag-SPANI, the peaks observed at 621 cm^{-1} and 705 cm^{-1} represent C-S and S-O bonds stretching vibrations, respectively (Ref 20, 28). The out-of-plane C-H vibrations was observed at 821 cm^{-1}, whereas asymmetric and symmetric stretching vibrations of O = S = O are observed at 1311 cm^{-1} and 1143 cm^{-1}, respectively. The secondary amine (C-N-C) stretching vibration is noticed at 1303 cm^{-1}.

3.2 X-ray Diffraction Studies

Figure 2 shows the x-ray diffraction patterns of GO, rGO-Ag and different wt.% rGO-Ag-SPANI nanohybrids. Based on Bragg's equation, the diffraction peak at 11.2° resembles the well-organized layer structure of GO with a d-spacing of 8.09 Å (Ref 29). Reducing agent in the preparation of Ag-decorated GO composite partially reduces GO. The shift in GO diffraction peak from 11.2° to 23.4° with broadening is in agreement with the literature results of rGO (Ref 30). Also, peaks corresponding to Ag, 38.16°, 44.33°, 64.56° and 77.53° are observed in rGO-Ag nanocomposite. XRD pattern of rGO-Ag-SPANI nanohybrids is similar to rGO-Ag but with an extra peak at 27.77° indicating the presence of SPANI, which is in
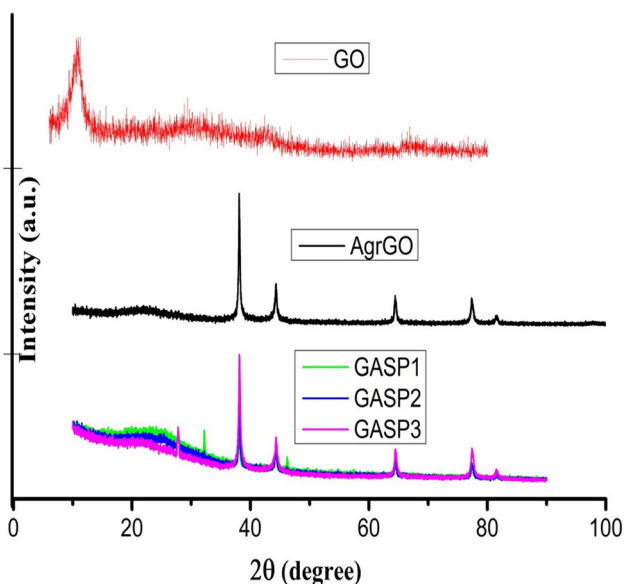
Fig. 2 XRD patterns of GO, rGO-Ag and different compositions of rGO-Ag-SPANI (GASP) nanocomposites

Fig. 3 Raman spectra of GO, rGO-Ag and rGO-Ag-SP

accordance with the literature data (Ref 29, 31). The XRD patterns of different wt.% of SPANI show that the increase in wt.% of SPANI results in decrease of rGO peak intensity but the intensity of the peak at 38° increases significantly, which enunciates the formation of rGO-Ag-SPANI nanohybrids. These results also suggested an increase in the interlayer spacing of GO by the interaction of Ag and SPANI with GO nanosheets.

3.3 Raman Spectral Studies

Raman spectra of GO, rGO-Ag and rGO-Ag-SPANI are displayed in Fig. 3. The two peaks observed between 2000 cm^{-1} and 1000 cm^{-1} are designated as G band and D band; while former represents the stretching vibration of the C-C bond in graphitic materials, the latter represents the structural disorder existing in the carbon-based materials (Ref 20). In the spectrum of GO, the D band and G band was characterized by the presence of peaks at 1345 cm^{-1} and 1592 cm^{-1}, respectively. Likewise, the D and G bands were observed at 1354 cm^{-1} and 1601 cm^{-1} for rGO-Ag and at 1349 cm^{-1} and 1599 cm^{-1} for rGO-Ag-SPANI, respectively. The intensity ratio of D to G peak (I_D/I_G) provides an effective method to calculate the degree of disorder and defects within the carbon nanomaterials. The intensity ratio of GO is 0.94, while that of rGO-Ag is 1.144. The deposition of Ag on GO and partial reduction of GO may be the reason for increased intensity in case of rGO-Ag (Ref 32). The I_D/I_G value of rGO-Ag-SPANI was estimated to be 1.034. The small decrement in this ratio may be attributed to the fact that, during *in situ* polymerization, SPANI may have formed by non-covalent interaction with the residual oxygen bearing groups of rGO, which mask the defect sites of rGO-Ag.

3.4 Contact Angle Analysis

Contact angle analysis is one of the most recognized tests of surface modification performed by the sessile drop method. The water contact angle analysis on top of the coatings was measure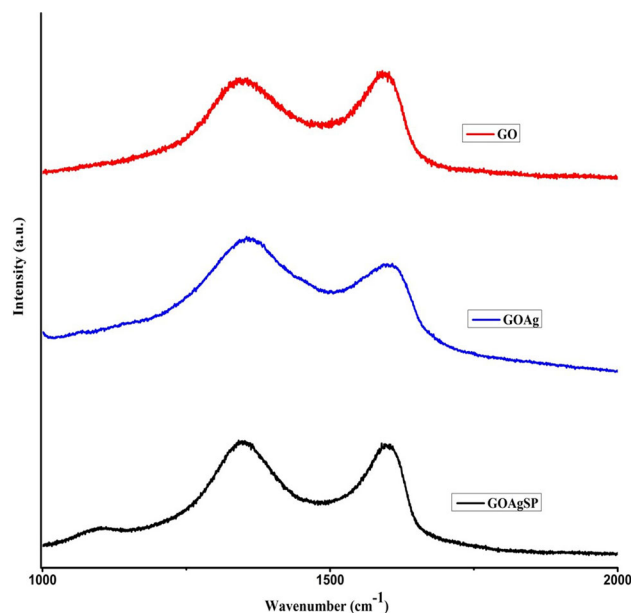d to examine the hydrophobicity of the coatings. A higher contact angle implies enhanced corrosion resistance, which restricts the access of surface of the coated specimen to the corrosive medium (Ref 33). The contact angle images of the coated samples are shown in Fig. 4. The rGO-Ag-SPANI-reinforced epoxy coating has a higher contact angle compared to that of pure epoxy coating, illustrating higher hydrophobicity and barrier properties. This increase in hydrophobicity is accorded to the increase in the degree of crosslinking (Ref 34).

3.5 SEM Analysis

The surface morphology of rGO-Ag-SPANI nanohybrid was examined by SEM analysis. SEM images of crumpled, well-dispersed (in ethanol) and dried rGO-Ag-SPANI are shown in Fig. 5(a-d). From these images, it can be seen that the SPANI has well covered the Ag-decorated GO sheets. Figure 5(e and f) shows the SEM images of the rGO-Ag-SPANI-2 + EP (GASP-2) nanocomposite-coated MS specimen. The uniform dispersion of nanocomposite in the epoxy matrix is seen in these images with chain-like linkages which interconnect the nanofiber structures (Ref 35). Figure 5(e) displays that uniform smooth surface on the MS specimen is formed by the nanocomposite coating. The magnified image of Fig. 5(e) shown in Fig. 5(f) determines that the rGO-Ag-SPANI exhibits excellent dispersibility with interfacial interaction in the epoxy matrix possessing less number of cracks (Ref 36).

3.6 Atomic Force Microscopy

AFM analysis provides information on surface morphology and the roughness of the GASP nanocomposite coating on the MS surface. AFM images also reflect the defects in the coatings such as pinholes and microcracks. Figure 6(a-f) shows the 2D, 3D topographical features and roughness parameters of the epoxy-coated and GASP-coated MS specimens, respectively. From Fig. 6(c), epoxy coating exhibits hills and valleys, whereas the GASP nanocomposite coating (Fig. 6d) shows uniform surface morphology. From Fig. 6(e, f), it can be seen that the roughness for the EP-coated sample is higher than that of GASP-coated MS sample. The average roughness (R_a) and
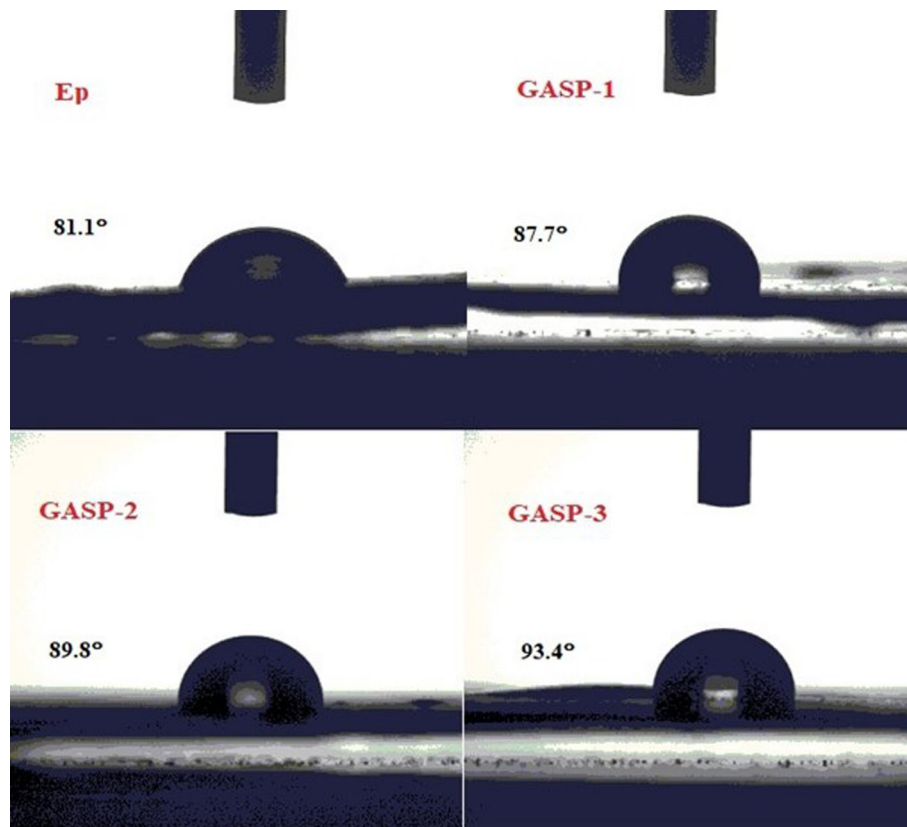
Fig. 4 Contact angle images of EP, GASP-1, GASP-2 and GASP-3

root mean square roughness (R_q) of GASP-3 and EP-coated MS samples were estimated to be 14.5 nm, 17.1 nm, and 17.3 nm, 20.5 nm, respectively. Since the surface roughness has significant influence on the coating adhesion and wear resistance, the addition of rGO-Ag/SPANI into the EP matrix has considerably decreased the surface roughness which in turn increases the adhesion and wear resistance properties of the coating (Ref 18, 37). Further, the thicknesses of the coatings were done on three replications of each sample. The average thickness of all the coated samples was estimated to be $32 \pm 0.5\ \mu m$.

3.7 TEM Analysis

The TEM images of rGO-Ag-SPANI nanohybrids at different magnifications are depicted in Fig. 6. The nanoscale images clearly show the decoration of SPANI on the surface of rGO-Ag nanosheets. Figure 7(a) clearly shows the deposition of silver nanoparticles on the surface of rGO sheet. Figure 7(b-e) displays that the SPANI moiety was decorated on the single sheet of rGO-Ag and globular type of structure formed by SPANI on the rGO-Ag surface might be because of the formation of the non-covalent bonding with the residual oxygen-containing groups of the rGO (Ref 38, 39). Figure 7f displays the size of the Ag nanoparticle decorated on the surface of rGO.

3.8 Corrosion Studies

3.8.1 Electrochemical Impedance Measurement. The effect of rGO-Ag-SPANI nanofiller on the anti-corrosion and barrier performance of epoxy coating on the MS surface in the

neutral saline medium was investigated through impedance measurement. The coated MS specimens with $1 cm^2$ active electrode surface area were immersed in 3.5 wt.% NaCl solution, and the open-circuit potential (OCP) was recorded before proceeding to EIS analysis. Figure 7 represents the plot of OCP vs time for different immersion times in 3.5 wt.% NaCl solution. The OCP values tend to drop on prolonged immersion, indicating that the specimen undergoes corrosion because of the diffusion of corrosive electrolytes into the coating–metal interface (Ref 40). From Fig. 8, it can be seen that GASP coating with the higher percentage of SPANI exhibits more positive values of OCP compared to that with a lower percentage of SPANI, indicating that the nanofillers have efficiently blocked or prevented the diffusion of corrosive electrolytes.

The coated and the uncoated MS specimens were subjected to EIS studies to understand the anti-corrosion behavior of rGO-Ag-SPANI in epoxy matrix. The Nyquist plots under room temperature for blank, epoxy-coated and different proportions of GASP-coated samples in 3.5 wt.% NaCl solution are displayed in Fig. 9. Nyquist data depict the complex plain diagram, where the impedance of the real component is plotted against the impedance of the imaginary (Ref 37). From Nyquist plot it is evident that the GASP-coated samples have the largest capacitance loops compared to EP and blank MS samples, while in the first day of immersion, a single loop is displayed by the GASP-coated samples, meaning that the corrosion-resistant property of coatings is directly related to the diameter of the semicircular Nyquist plot. The significant increase in diameter of semicircles with the increase in percentage composition of SPANI in the GASP expresses that rGO-Ag-
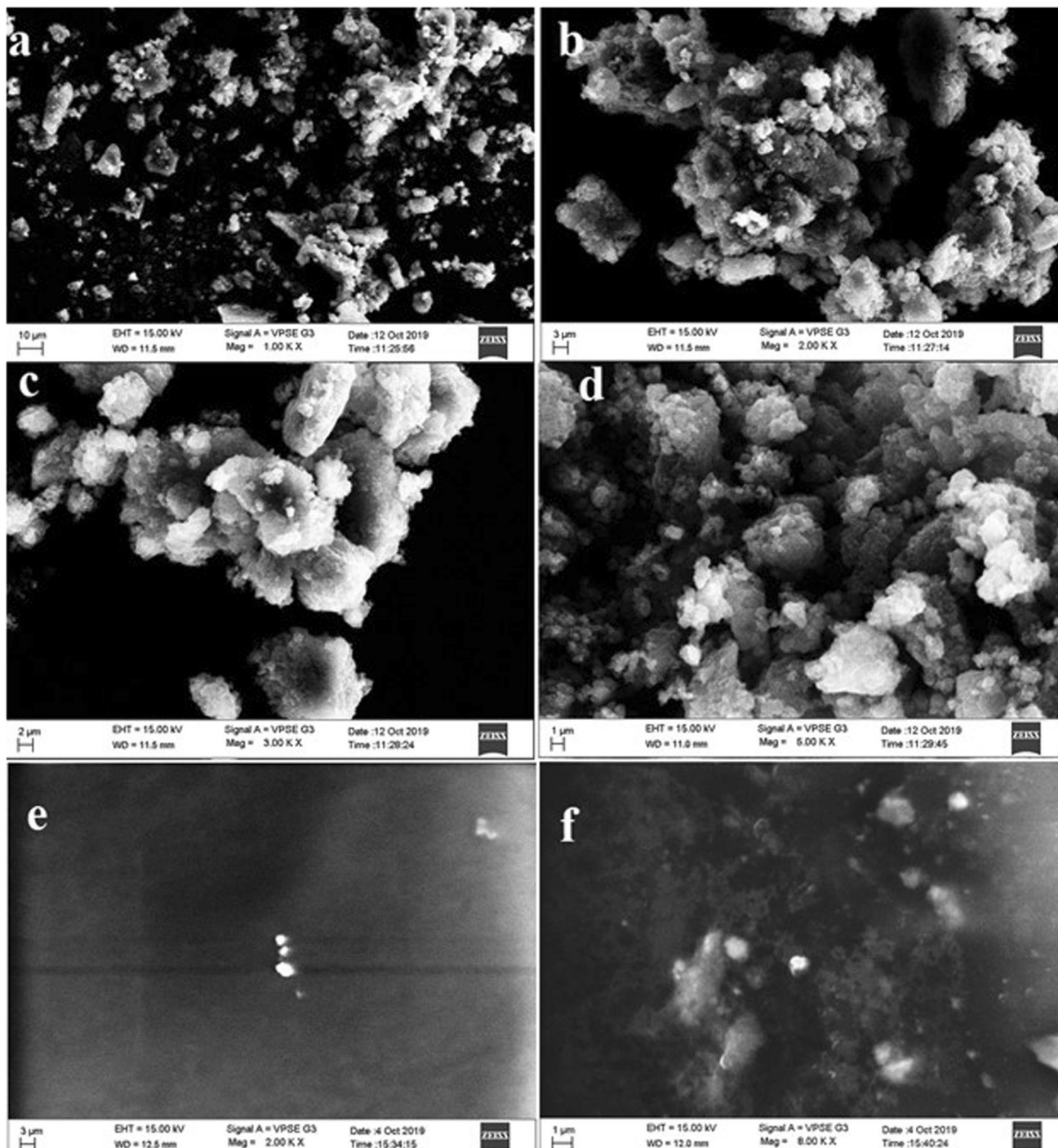
Fig. 5 SEM micrographs of (a-d) powder rGO-Ag-SPANI and (e, f) GASP-coated MS samples

SPANI nanocomposites can increase the corrosion inhibition performance of the pure EP resin. But the capacitive loops are not perfect semicircles (Ref 41). Hence, the double-layer capacitance will not function as an ideal capacitor, so the constant phase element is established.

The equivalent electrical circuit employed to get the replicate model of impedance data is shown in Fig. 10. The data produced using the electrical circuit are in good agreement with the experimental results. Here R_s, Q_{dl}, R_c, Q_{ct} and R_{ct} refer to the solution resistance, double-layer constant phase element,
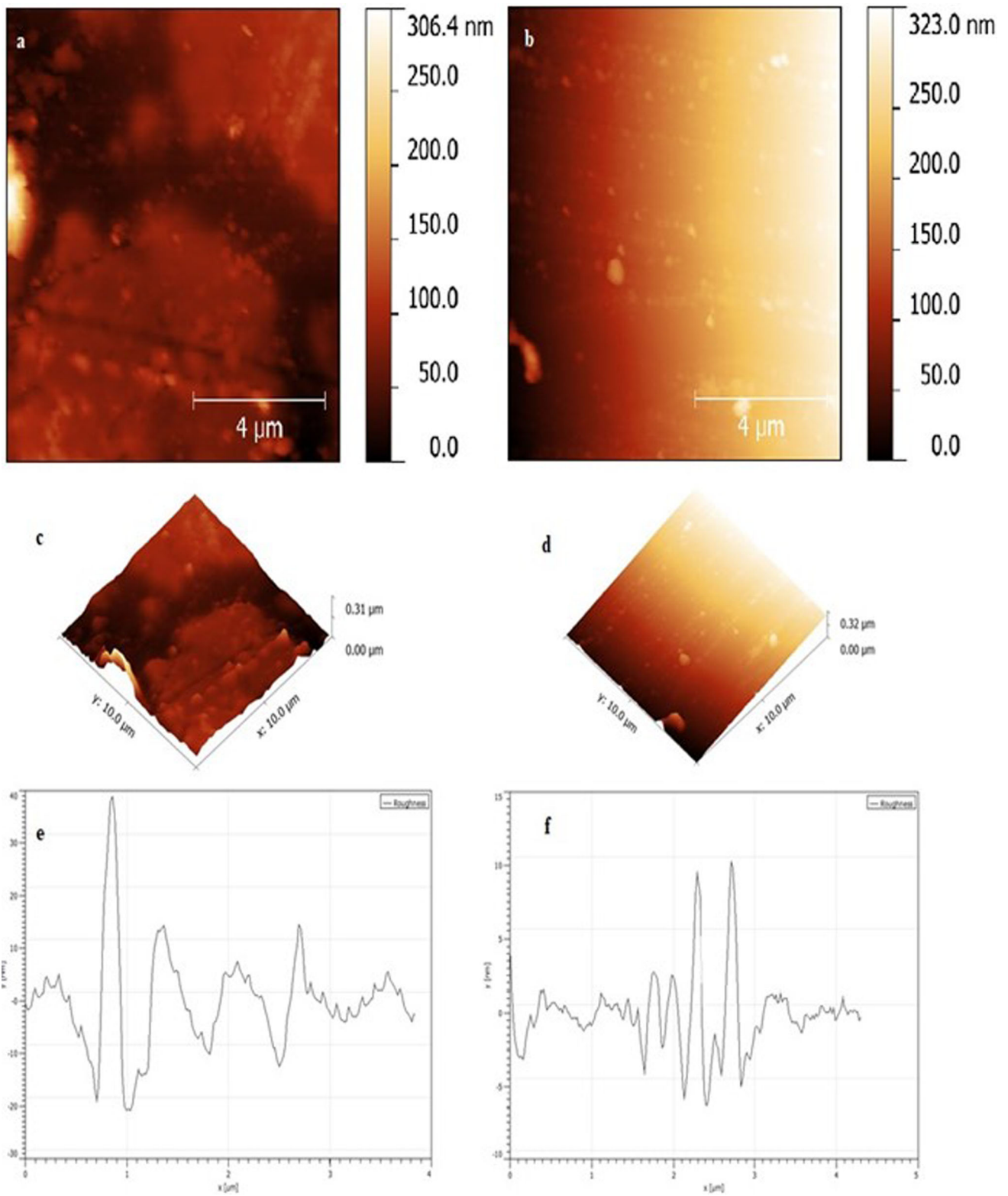
Fig. 6 AFM images of EP and GASP coating (a, b) 2D, (c, d) 3D and (e, f) roughness
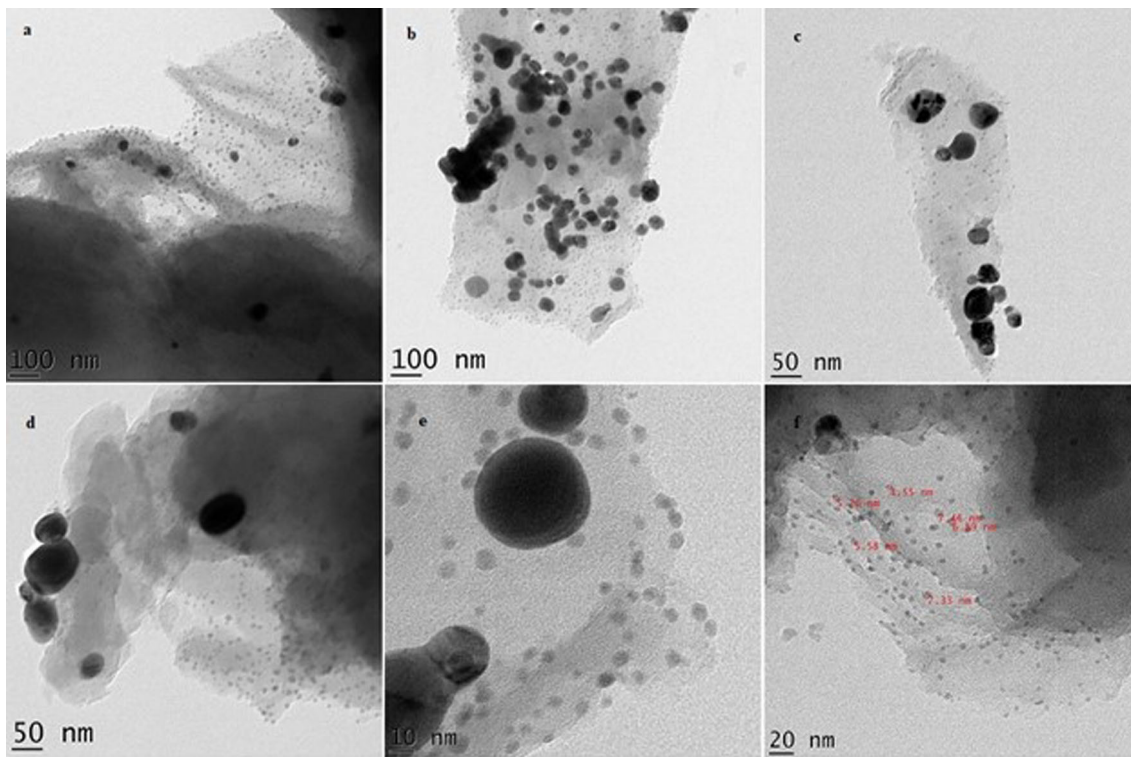
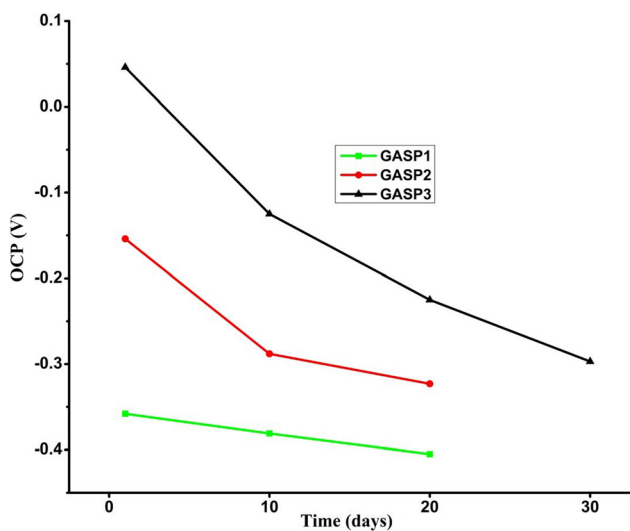**Fig. 7** TEM morphologies of powder rGO-Ag-SPANI

Fig. 8 OCP vs time plots of different wt.% of SPANI-incorporated GASP nanocomposite-coated MS immersed in 3.5 wt.% NaCl solution

coating resistance, charge transfer constant phase element and charge transfer resistance, respectively. The impedance of the constant phase element, Z_{CPE}, can be expressed by equation (1).

$$Z_{CPE} = \frac{1}{Y_o(j\omega)^n} \quad \text{(Eq 1)}$$

where Y_o represents CPE constant, j is imaginary constant and n is CPE exponent (where $0 < n < 1$).

R_c and R_{ct} values increase with higher percentage of SPANI in GASP (GASP-3); this may be ascribed due to the bonding of SPANI with rGO-Ag which blocks the intrusion of aggressive electrolytes to permeate the coating. The nanosized silver decorated on graphene oxide can block the porous structure of EP and protect the metal from corrosive electrolytes, but ensures electron transfer, thereby acting as an additional passive barrier for the movement of electrolytes through the diffusion path. The larger size of silver atom than sodium ion ensures the effective blockade of ion and hence prevents corrosion. It clearly indicates that the incorporation of rGO-Ag-SPANI nanofillers increases the barrier properties of the EP matrix. Therefore, hydrophobicity, better adhesion, barrier properties of GASP coatings and also formation of corrosion products suppress the corrosive electrolytes diffusion through the coating. The diameter of the capacitive loops decreases with increase in immersion time (Ref 42). Figure 9(b) clearly indicates that GASP-3 coating has the largest capacitive loop compared to that of GASP-1 and GASP-2 coatings after 10 days of immersion. The same trend follows for 20th and 30th days of immersion, but the diameter of the semicircle decreased significantly. As the immersion time increases, the corrosive electrolytes make a pathway to somehow reach the metal-coating interface. The corresponding results are given in Table 2.

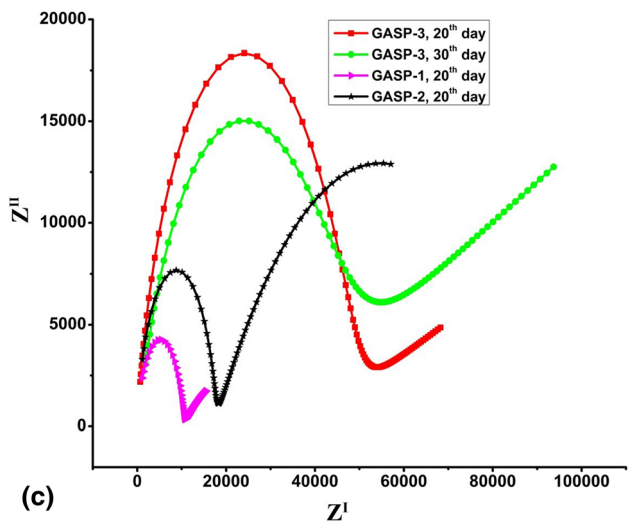The Bode plots of the GASP-coated specimens are depicted in Fig 11. GASP-3-coated sample shows high impedance at lower frequency ($|Z|_{0.01\ Hz}$) and high phase angle at higher frequency ($\theta_{0.1\ MHz}$) initially compared to GASP-1 and GASP-
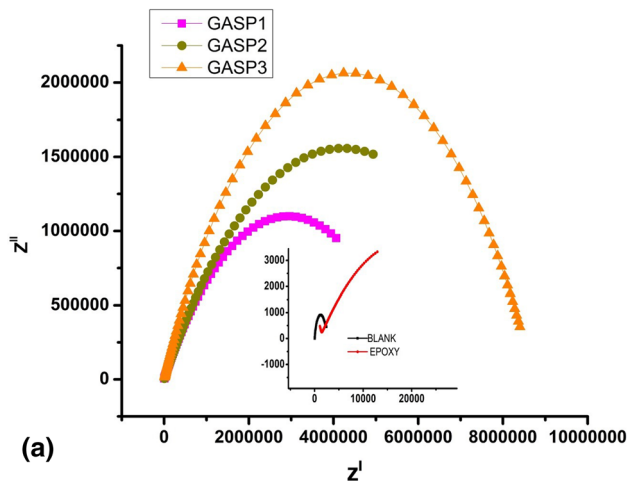
(a)
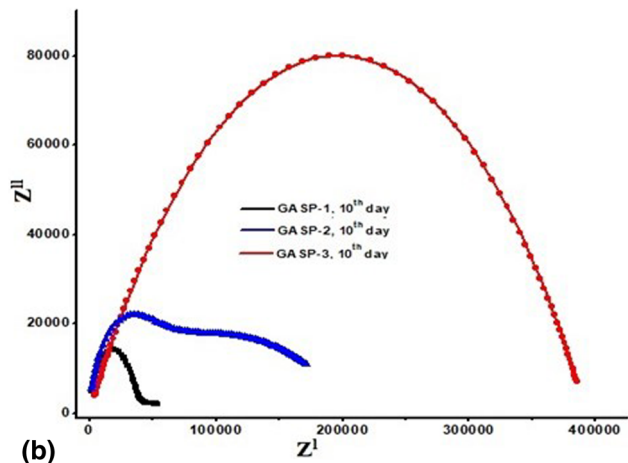
(b)

(c)

Fig. 9 (a) Nyquist plots of blank, epoxy and different wt.% of SPANI-incorporated GASP nanocomposite-coated MS after 24 hrs of immersion in 3.5 wt.% NaCl solution. (b) Nyquist plots of different wt.% of SPANI-incorporated GASP nanocomposite-coated MS after 10 days of immersion in 3.5 wt.% NaCl solution. (c) Nyquist plot of different wt.% of SPANI-incorporated GASP nanocomposite-coated MS after 20th day of immersion in 3.5 wt.% NaCl solution
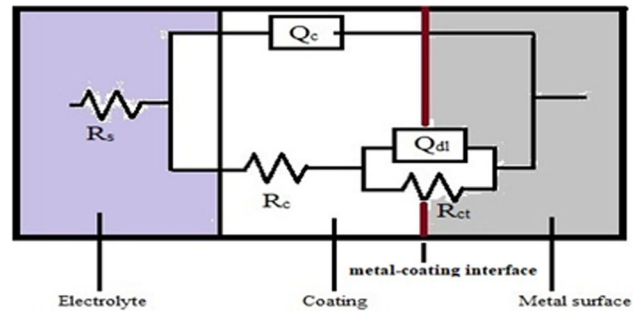

Fig. 10 Fitted equivalent electrical circuit

2 coatings. It signifies that GASP-3 shows a good barrier performance against the corrosive electrolyte and in turn protection from corrosion. All the GASP-coated samples exhibit $|Z|_{0.01 \text{ Hz}}$ values in the order of 10^6 Ω. cm^2. After 10 days of immersion, GASP-3 shows the highest value of $|Z|_{0.01 \text{ Hz}}$ with the order of 10^5 Ω. cm^2 when compared to GASP-2 and GASP-1. This shows that GASP has significantly prevented the sample from undergoing corrosion. As the immersion time increases to 20 days, a significant decrease in $|Z|_{0.01 \text{ Hz}}$ values of GASP-1 and GASP-2 is observed, while that of GASP-3 decreased moderately compared to 10th day of immersion because of the newer diffusion paths created by the electrolytes. After 20 days of immersion, delamination is identified in GASP-1 and GASP-2 coatings, while the GASP-3 coating is still intact on the surface of the sample. But in between 20 and 30 days of immersion, delamination of GASP-3 is also observed, resulting in the formation of corrosion products on the specimen. The higher value of $|Z|_{0.01 \text{ Hz}}$ for GASP-3 nanocomposite throughout immersion time displays, more stable coating has been achieved by incorporating SPANI with rGO-Ag.

Figure 11 displays the phase angle curves of the GASP-1, GASP-2 and GASP-3 nanocomposite-coated MS in 3.5 wt.% NaCl solution during initial immersion. Generally, the response of coating is assigned to peak at higher frequencies (10^4 - 10^5 Hz), response of the coating defects is observed in medium frequencies (100 -10^3 Hz), and the characteristic response of the MS corrosion is found at low frequencies (10^{-2}-100 Hz) (Ref 22). The phase angle at higher frequency ($\theta_{0.1 \text{ MHz}}$) also gives insight in estimating the anti-corrosion performance of coatings. Results from the graph show that GASP-3 has the highest value of phase angle at 83°, whereas that of GASP-1 and GASP-2 is 56° and 66°, respectively. It shows that incorporation of SPANI-decorated rGO-Ag into the epoxy matrix helps in denying the diffusion of corrosive electrolyte through the coating. The larger phase angle values for GASP coatings with higher proportion of SPANI indicate its superior protection efficiency. After 10 days of immersion, the $\theta_{0.1 \text{ MHz}}$ decreases very slightly, showing that the GASP coating is still offering blockade to the pathways of the corrosive electrolyte in reaching metal/coating interface. But after 20 days of immersion, $\theta_{0.1 \text{ MHz}}$ of GASP-1 and GASP-2 decreases significantly compared to GASP-3. Therefore, from Bode plot, it is again

Table 2 The electrochemical parameters obtained by fitting EIS equivalent circuit for blank, EP- and GASP-coated MS samples in 3.5 wt.% NaCl solution

| Sample	Q_c		R_c	Q_{dl}		R_{ct}
	Y_o, Ω^{-1} cm^{-2} s^n	n	Ω cm^2	Y_o, Ω^{-1} cm^{-2} s^n	n	Ω cm^2
Blank	6.247×10^{-6}	0.391	6.605×10^{2}	4.396×10^{-5}	0.781	9.417×10^{2}
EP	2.354×10^{-7}	0.641	2.683×10^{4}	5.221×10^{-6}	0.744	1.087×10^{4}
GASP-1						
1st day	2.940×10^{-7}	0.457	2.38×10^{6}	4.644×10^{-7}	0.985	5.86×10^{6}
10th day	1.945×10^{-6}	0.868	1.718×10^{5}	7.909×10^{-6}	0.070	8.334×10^{4}
20th day	3.604×10^{-5}	0.875	1.025×10^{4}	2.916×10^{-4}	0.269	2.214×10^{4}
GASP-2						
1st day	3.047×10^{-7}	0.451	8.429×10^{6}	1.071×10^{-7}	0.040	1.916×10^{6}
10th day	2.034×10^{-6}	0.205	7.471×10^{5}	9.177×10^{-6}	0.915	2.132×10^{5}
20th day	1.648×10^{-6}	0.914	1.742×10^{4}	3.878×10^{-5}	0.425	7.461×10^{4}
GASP-3						
1st day	3.079×10^{-8}	0.563	8.717×10^{7}	2.905×10^{-8}	0.738	2.170×10^{7}
10th day	2.646×10^{-7}	0.493	4.736×10^{7}	5.78×10^{-7}	0.003	7.151×10^{6}
20th day	6.694×10^{-6}	0.841	3.834×10^{6}	4.385×10^{-6}	0.103	9.745×10^{5}
30th day	1.287×10^{-6}	0.760	2.975×10^{6}	2.185×10^{-5}	0.126	1.993×10^{5}
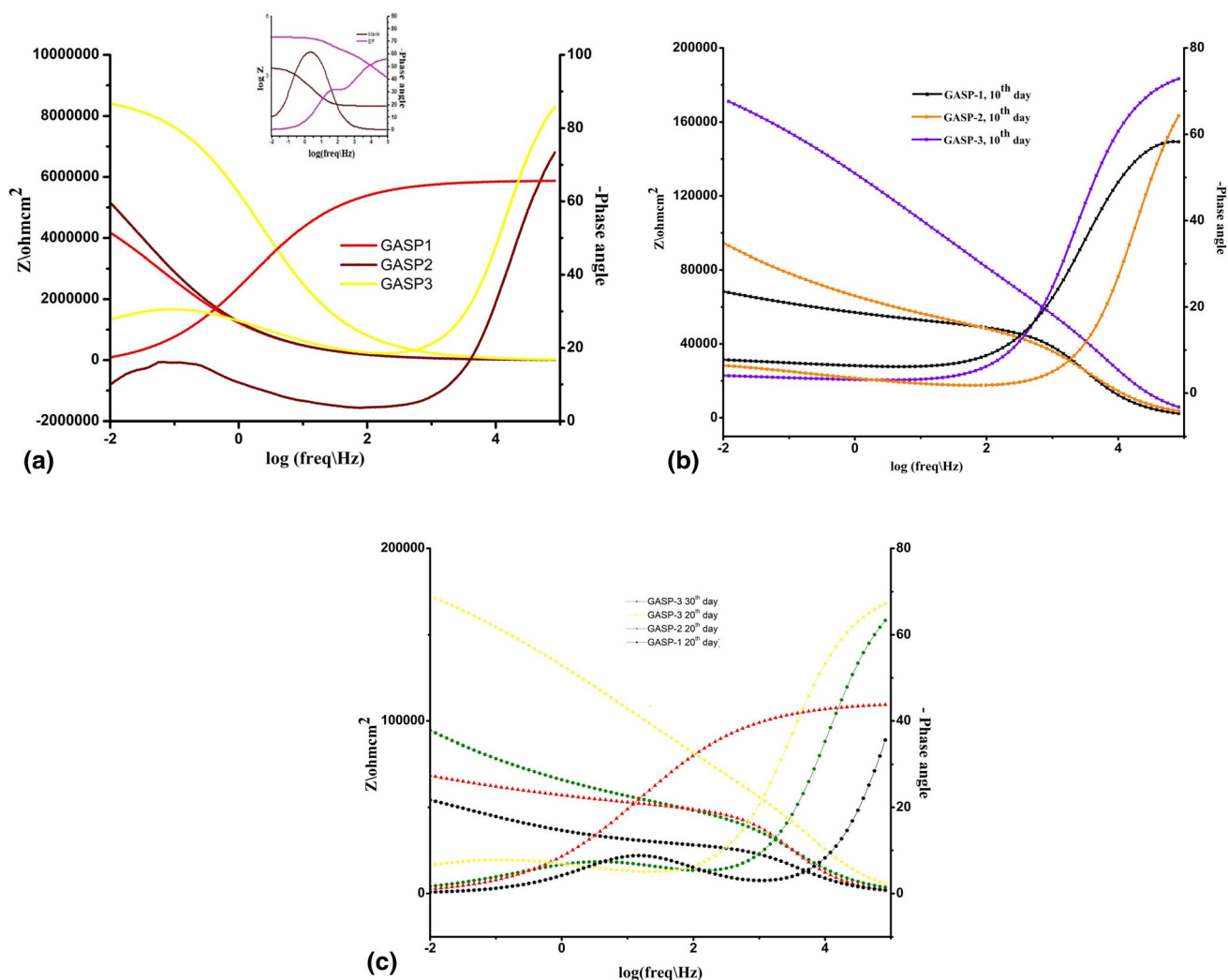
Fig. 11 (a) Bode plots of blank, epoxy and different wt.% of SPANI-incorporated GASP nanocomposite-coated MS after 24 hrs of immersion in 3.5 wt.% NaCl solution. (b) Bode plots of different wt.% of SPANI-incorporated GASP nanocomposite-coated MS after 10 days of immersion in 3.5 wt.% NaCl solution. (c) Bode plots of different wt.% of SPANI-incorporated GASP nanocomposite-coated MS after 20 days of immersion in 3.5 wt.% NaCl solution

Table 3 Polarization parameters for blank, EP- and GASP-coated MS samples in 3.5 wt.% NaCl solution

Sample	E_{corr}, V	i_{corr}, A/cm^2	b_c, V/dec	b_a, V/dec	CR, Angs/min
Blank	− 0.594	2.328×10^{-6}	10.227	11.406	5.120×10^{-1}
EP	− 0.429	7.155×10^{-7}	3.544	5.888	1.573×10^{-1}
GASP-1					
1st day	− 0.334	1.043×10^{-8}	6.049	5.655	9.851×10^{-2}
10th day	− 0.405	2.703×10^{-6}	5.086	4.904	5.944×10^{-1}
20th day	− 0.428	9.903×10^{-5}	5.126	5.080	8.583×10^{-1}
GASP-2					
1st day	− 0.202	9.314×10^{-8}	6.094	5.202	2.048×10^{-3}
10th day	− 0.298	1.826×10^{-7}	4.901	5.040	4.016×10^{-2}
20th day	− 0.372	1.090×10^{-6}	4.823	6.297	2.397×10^{-1}
GASP-3					
1st day	− 0.001	4.050×10^{-9}	5.017	5.154	8.905×10^{-4}
10th day	− 0.225	9.578×10^{-7}	5.046	4.760	3.064×10^{-3}
20th day	− 0.245	3.653×10^{-7}	5.151	4.803	8.034×10^{-2}
30th day	− 0.306	5.909×10^{-6}	5.704	4.871	1.299×10^{-1}

evident that GASP-3 coating shows superior corrosion resistance performance and excellent barrier properties (Ref 43).

3.8.2 Potentiodynamic Polarization Studies. The Tafel polarization curves of GASP-coated MS specimens immersed in 3.5 wt.% NaCl solution are displayed in Fig. 12. In general, higher values of E_{corr} and lower I_{corr} values signify excellent corrosion prevention. After 24 hrs of immersion (Fig. 12a), a shift toward more positive potential is observed for all the three GASP-coated samples when compared to blank and EP, whereas the corrosion current densities moved drastically toward lower values. From the Tafel plots, it is observed that GASP-3 coating has the highest E_{corr} than GASP-2 and GASP-1. The corrosion current densities of the GASP-coated samples reduced and followed the order $I_{corr\ (GASP-1)} > I_{corr\ (GASP-2\%)} > I_{corr\ GASP-3}$. The rate of corrosion of the samples can be obtained from I_{corr} using equation (2).

$$CR = \frac{kMI_{corr}}{n\rho} \qquad (Eq\ 2)$$

where k is constant, M is the atomic weight of metal (g/mol), n is the number of charge transfer and ρ is the density of metal (g/cm^3) (Ref 34).

After 10 days of immersion, E_{corr} for GASP-coated samples decreases marginally and that of I_{corr} increases slightly, which signifies infiltration of corrosive electrolyte to the metal-coating interface. Further from the polarization data, it is also evident that GASP-3-coated samples are least affected by the corrosive electrolytes when compared to GASP-1 and GASP-2 coatings. This can be ascribed to the presence of a greater number of polymer molecules in coating, which blocks effectively the passage of corrosive electrolytes through the micropores of EP resin (Ref 44). After 20 and 30 days of immersion, the polarization results reinforce the trend observed by EIS data. The results obtained from polarization tests are given in Table 3.

4. Conclusion

In the present study, we synthesized silver-decorated reduced graphene oxide/sulfonated polyaniline nanohybrid was synthesized and characterized by XRD, TEM, FT-IR and Raman spectral analyses. The surface characterization was done using SEM, contact angle and AFM studies. The decoration of silver nanoparticles on the surfaces of the graphene oxide sheets as well as the coating of the hybrid nanosheets by the polymer is evident from TEM images. This study explores the role of synthesized nanohybrid (rGO-Ag/SPANI) in improving the corrosion protection and barrier performance of the epoxy (EP) on mild steel (MS) in 3.5 wt.% NaCl medium. Higher percentage of SPANI in the composite increased the hydrophobicity of the nanocomposite coating. Electrochemical impedance spectroscopy and potentiodynamic polarization studies revealed the excellent barrier protection and anti-corrosion performance for the nanocomposite coatings having higher percentage of SPANI. Also, it showed good stability up to 30 days of the coating by increasing the pathway of the electrolyte to the metal surface by blocking the pores in the EP.
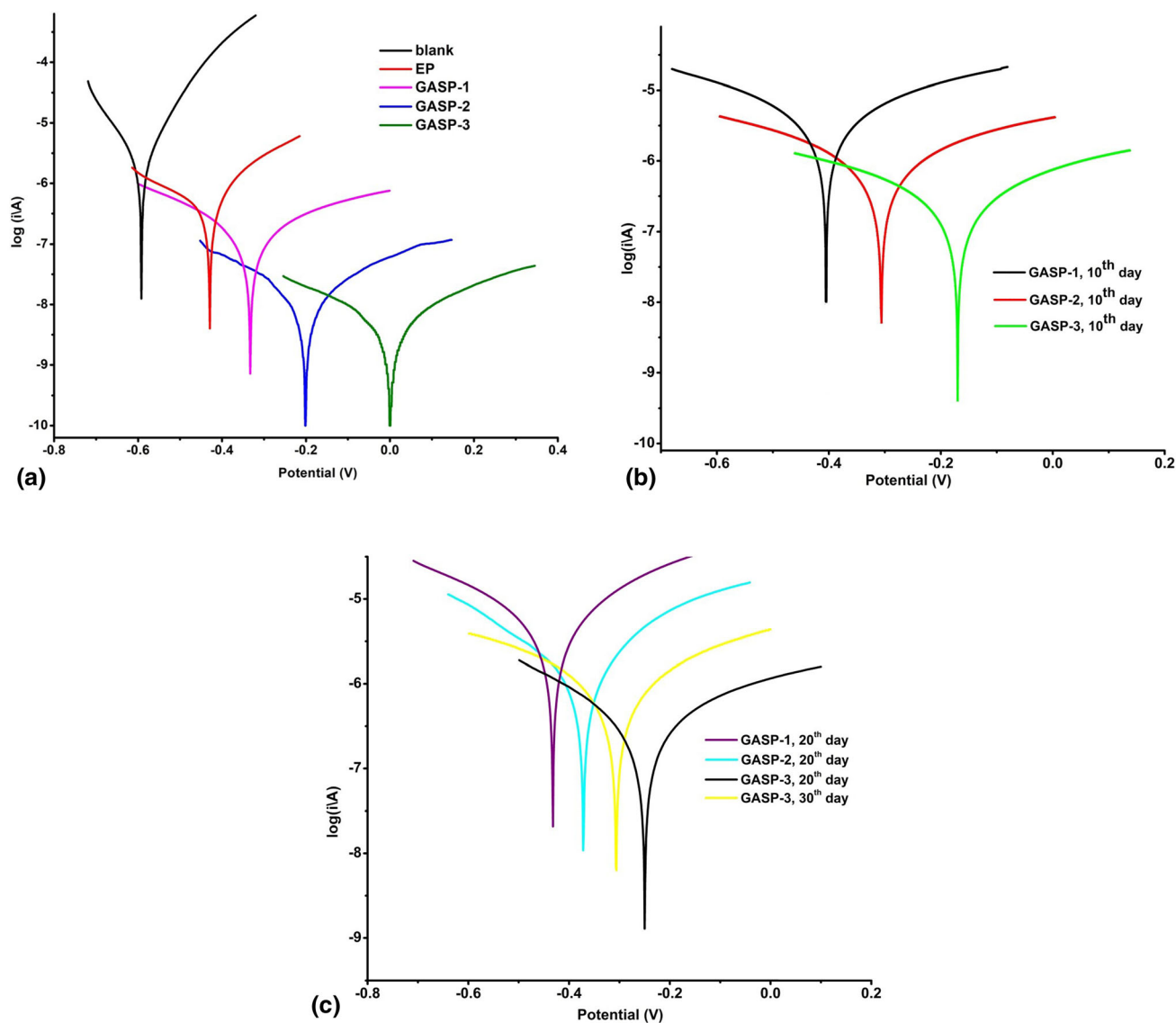
Fig. 12 (a) Tafel plots of blank, epoxy and different wt.% of SPANI-incorporated GASP nanocomposite-coated MS after 24 h of immersion in 3.5 wt.% NaCl solution. (b) Tafel plots of different wt.% of SPANI-incorporated GASP nanocomposite-coated MS after 10 days of immersion in 3.5 wt.% NaCl solution. (c) Tafel plots of different wt.% of SPANI-incorporated GASP nanocomposite-coated MS after 20 days of immersion in 3.5 wt.% NaCl solution.

Reference

1. C.X. Wang and X.F. Zhang, A Non-particle and Fluorine-Free Superhydrophobic Surface Based on One-Step Electrodeposition of Dodecyltrimethoxysilane on Mild Steel for Corrosion Protection, *Corros. Sci.*, 2019, **163**, 108284. https://doi.org/10.1016/j.corsci.2019.108284

2. A. Dehghani, F. Poshtiban, and G. Bahlakeh, Fabrication of Metal-Organic Based Complex Film Based on Three-Valent Samarium Ions-[bis (phosphonomethyl) amino] Methylphosphonic Acid (ATMP) for Effective Corrosion Inhibition of Mild Steel in Simulated Seawater, *Constr. Build. Mater.*, 2020, **239**, p 17812. https://doi.org/10.1016/j.conbuildmat.2019.117812

3. A.A.M.M. Singh, P.A. Franco, and J.S. Binoj, Enhancement of Corrosion Resistance on Plasma Spray Coated Mild Steel Substrate Exposed to Marine Environment, *Mater. Today*, 2019, **15**, p 84–89. https://doi.org/10.1016/j.matpr.2019.05.028

4. S. Karthick, S. Muralidharan, and V. Saraswathy, Corrosion Performance of Mild Steel and Galvanized Iron in Clay Soil Environment, *Arab. J. Chem.*, 2020, **13**(1), p 3301–3318. https://doi.org/10.1016/j.arabjc.2018.11.005

5. M.G. Sari, B. Ramezanzadeh, M. Shahbazi, and A.S. Pakdel, Influence of Nanoclay Particles Modification by Polyester-Amide Hyper-branched Polymer on the Corrosion Protective Performance of the Epoxy Nanocomposite, *Corros. Sci.*, 2015, **92**, p 162–172. https://doi.org/10.1016/j.corsci.2014.11.047

6. K. Patel, R. Singh, and H.W. Kim, Carbon Based-Nanomaterials as an Emerging Platform for Theranostics, *Mater. Horiz.*, 2018, **6**, p 434–469. https://doi.org/10.1039/c8mh00966j

7. R. Rauti, M. Musto, S. Bosi, M. Prato, and L. Ballerini, Properties and Behavior of Carbon Nanomaterials When Interfacing Neuronal Cells: How Far Have We Come?, *Carbon*, 2018 https://doi.org/10.1016/j.carbon.2018.11.026

8. I. Khan, K. Saeed, and I. Khan, Nanoparticles: Properties, Applications and Toxicities, *Arab. J. Chem.*, 2017, **12**(7), p 908–931. https://doi.org/10.1016/j.arabjc.2017.05.011

9. G. Cui, Z. Bi, R. Zhang, J. Liu, and XYu.Z. Li, A Comprehensive Review on Graphene-Based Anti-Corrosive Coatings, *Chem. Eng. J.*, 2019, **2019**(373), p 104–121. https://doi.org/10.1016/j.cej.2019.05.034

10. A.A. Olajire, Recent Advances on Organic Coating System Technologies for Corrosion Protection of Offshore Metallic Structures, *J. Mol.*

Liq., 2018, **269**, p 572–606. https://doi.org/10.1016/j.molliq.2018.08.053

11. Y. Ahmadi and S. Ahmad, Surface-Active Antimicrobial and Anticorrosive Oleo-Polyurethane/Graphene Oxide Nanocomposite Coatings: Synergistic Effects of In-Situ Polymerization and π-π Interaction, *Prog. Org. Coat.*, 2019, **127**, p 168–180. https://doi.org/10.1016/j.porgcoat.2018.11.019

12. S. Amrollahi, B. Ramezanzadeh, H. Yari, M. Ramezanzadeh, and M. Mahdavian, Synthesis of Polyaniline-Modified Graphene Oxide for Obtaining a High Performance Epoxy Nanocomposite Film with Excellent UV Blocking/Anti-Oxidant/Anti-Corrosion Capabilities, *Compos. Part B-Eng.*, 2019, **173**, 106804. https://doi.org/10.1016/j.compositesb.2019.05.015

13. Q. Zhu, E. Li, X. Liu, W. Song, Y. Li, X. Wang, and C. Liu, Epoxy Coating with in-Situ Synthesis of Polypyrrole Functionalized Graphene Oxide for Enhanced Anticorrosive Performance, *Prog. Org. Coat.*, 2020, **140**, 105488. https://doi.org/10.1016/j.porgcoat.2019.105488

14. A.A. Javidparvar, R. Naderi, and B. Ramezanzadeh, Epoxy-Polyamide Nanocomposite Coating with Graphene Oxide as Cerium Nanocontainer Generating Effective Dual Active/Barrier Corrosion Protection, *Compos. Part B-Eng.*, 2019, **172**, p 363–375. https://doi.org/10.1016/j.compositesb.2019.05.055

15. M. Ramezanzadeh, B. Ramezanzadeh, M.G. Sari, and M.R. Saeb, Corrosion Resistance of Epoxy Coating on Mild Steel Through Polyamidoamine Dendrimer-Covalently Functionalized Graphene Oxide Nanosheets, *J. Ind. Eng. Chem.*, 2019, **82**, p 290–302. https://doi.org/10.1016/j.jiec.2019.10.025

16. M.G. Sari and B. Ramezanzadeh, Epoxy Composite Coating Corrosion Protection Properties Reinforcement Through the Addition of Hydroxyl-Terminated Hyperbranched Polyamide Non-Covalently Assembled Graphene Oxide Platforms, *Constr. Build. Mater.*, 2020, **234**, 117421. https://doi.org/10.1016/j.conbuildmat.2019.117421

17. S.R. Nayak and K.N.S. Mohana, Corrosion Protection Performance of Functionalized Graphene Oxide Nanocomposite Coating on Mild Steel, *Surf. Interfaces*, 2018, **11**, p 63–73. https://doi.org/10.1016/j.surfin.2018.03.002

18. K. Rajitha and K.N.S. Mohana, Application of Modified Graphene Oxide – Polycaprolactone Nanocomposite Coating for Corrosion Control of Mild Steel in Saline Medium, *Mater. Chem. Phy.*, 2019, **241**, 122050. https://doi.org/10.1016/j.matchemphys.2019.122050

19. G. Liao, Y. Gong, C. Yi, and Z. Xu, Soluble, Antibaterial, and Anticorrosion Studies of Sulfonated Polystyrene/Polyaniline/Silver Nanocomposites Prepared with the Sulfonated Polystyrene Template, *Chin. J. Chem.*, 2017, **35**(7), p 1157–1164. https://doi.org/10.1002/cjoc.201600816

20. C. Zhou, M. Hong, Y. Yang, N. Hu, Z. Zhou, L. Zhang, and Y. Zhang, Engineering Sulfonated Polyaniline Molecules on Reduced Graphene Oxide Nanosheets for High-Performance Corrosion Protective Coatings, *Appl. Surf. Sci.*, 2019, **484**, p 663–675. https://doi.org/10.1016/j.apsusc.2019.04.067

21. S. Qiu, C. Chen, W. Zheng, W. Li, H. Zhao, and L. Wang, Long-Term Corrosion Protection of Mild Steel by Epoxy Coating Containing Self-Doped Polyaniline Nanofiber, *Synth. Metals*, 2017, **229**, p 39–46. https://doi.org/10.1016/j.synthmet.2017.05.004

22. Y. Hayatgheib, B. Ramezanzadeh, P. Kardar, and M. Mahdavian, A Comparative Study on Fabrication of a Highly Effective Corrosion Protective System Based on Graphene Oxide-Polyaniline Nanofibers/Epoxy Composite, *Corros. Sci.*, 2018, **133**, p 358–373. https://doi.org/10.1016/j.corsci.2018.01.046

23. C. Jeyaprabha, S. Sathiyanarayanan, and G. Venkatachiari, Investigation of the Inhibitive Effect of Polyaniline on Corrosion of Iron in 05 M H2SO4 Solutions, *J. Electroanal. Chem.*, 2005, **583**, p 232–240

24. S. Pourhashem, E. Ghasemy, A. Rashidi, and M.R. Vaezi, Corrosion Protection Properties of Novel Epoxy Nanocomposite Coatings Containing Silane Functionalized Graphene Quantum Dots, *J. Alloys Compd.*, 2018, **731**, p 1112–1118

25. P. Du, S. Qiu, C.L. Guangzhou, L.H. Zhao, and L. Wang, In situ Polymerization of Sulfonated Polyaniline in Layered Double Hydroxide Host Matrix for Corrosion Protection, *New J. Chem.*, 2018, **42**, p 4201–4209

26. S. Chook, C. Chia, S. Zakaria, M. Ayob, K. Chee, N. Huang, H. Neoh, H. Lim, R. Jamal, and R. Rahman, Antibacterial Performance of Ag Nanoparticles and AgGO Nanocomposites Prepared via Rapid Microwave-Assisted Synthesis Method, *Nanoscale Res. Lett.*, 2012, **7**(1), p 541. https://doi.org/10.1186/1556-276x-7-541

27. Q. Wu, G.E. Chen, W.G. Sun, Z.L. Xu, Y.F. Kong, X.P. Zheng, and S.J. Xu, Bio-Inspired GO-Ag/PVDF/F127 Membrane with Improved Anti-Fouling for Natural Organic Matter (NOM) Resistance, *Chem. Eng. J.*, 2017, **313**, p 450–460. https://doi.org/10.1016/j.cej.2016.12.079

28. L.C. Mendes, A.P.S. Falco, M.S. Pinho, and P.O. Marques, Sulfonated Polyaniline: Influence of Sulfonation Routes on Its Thermal and Structural Characteristics, *Mater. Res.*, 2011, **14**(4), p 466–471. https://doi.org/10.1590/s1516-14392011005000070

29. H. Ilyas, S. Shawuti, M. Siddiq, J.H. Niazi, and A. Qureshi, PEG Functionalized Graphene Oxide-Silver Nano-Additive for Enhanced Hydrophilicity, Permeability and Fouling Resistance Properties of PVDF-co-HFP Membranes, *Colloids Surf. A*, 2019, **579**, 123646. https://doi.org/10.1016/j.colsurfa.2019.123646

30. J. Chen, X. Zheng, H. Wang, and W. Zheng, Graphene Oxide-Ag Nanocomposite: In Situ Photochemical Synthesis and Application as a Surface-Enhanced Raman Scattering Substrate, *Thin Solid Films*, 2011, **520**(1), p 179–185. https://doi.org/10.1016/j.tsf.2011.07.012

31. Y. Liao, V. Strong, W. Chian, X. Wang, X.G. Li, and R.B. Kaner, Sulfonated Polyaniline Nanostructures Synthesized via Rapid Initiated Copolymerization with Controllable Morphology, Size, and Electrical Properties, *Macromolecules*, 2012, **45**(3), p 1570–1579. https://doi.org/10.1021/ma2024446

32. A. Shaikh, S. Parida, and S. Böhm, One Step Eco-Friendly Synthesis of Ag–Reduced Graphene Oxide Nanocomposite by Phytoreduction for Sensitive Nitrite Determination, *RSC Adv.*, 2016, **6**(102), p 100383–100391. https://doi.org/10.1039/c6ra23655c

33. H. Jeon, J. Park, and M. Shon, Corrosion Protection by Epoxy Coating Containing Multi-Walled Carbon Nanotubes, *J. Ind. Eng. Chem.*, 2013, **19**(3), p 849–853. https://doi.org/10.1016/j.jiec.2012.10.030

34. K. Rajitha, K.N.S. Mohana, A. Mohanan, and A.M. Madhusudhana, Evaluation of Anti-Corrosion Performance of Modified Gelatin-Graphene Oxide Nanocomposite Dispersed in Epoxy Coating on Mild Steel in Saline Media, *Colloids Surf. A*, 2020, **587**, 124341. https://doi.org/10.1016/j.colsurfa.2019.124341

35. F. Yang, T. Liu, J. Li, S. Qiu, and H. Zhao, Anticorrosive Behavior of a Zinc-Rich Epoxy Coating Containing Sulfonated Polyaniline in 35% NaCl Solution, *RSC Adv.*, 2018, **8**(24), p 13237–13247. https://doi.org/10.1039/c8ra00845k

36. Z. Qi, Y. Tan, Z. Zhang, L. Gao, C. Zhang, and J. Tian, Synergistic Effect of Functionalized Graphene Oxide and Carbon Nanotube Hybrids on Mechanical Properties of Epoxy Composites, *RSC Adv.*, 2018, **8**(67), p 38689–38700. https://doi.org/10.1039/c8ra08312f

37. M.B. Hegde, S.R. Nayak, K.N.S. Mohana, and N. Kumaraswamy, Garcinia Gummigutta Vegetable Oil–Graphene Oxide Nano-Composite: An Efficient and Eco-Friendly Material for Corrosion Prevention of Mild Steel in Saline Medium, *J. Poly. Environ.*, 2020, **28**, p 483–499. https://doi.org/10.1007/s10924-019-01611-y

38. F. Soysal, Z. Çıplak, B. Getiren, C. Gökalp, and N. Yıldız, Synthesis of GO-Fe$_3$O$_4$-PANI Nanocomposite with Excellent NIR Absorption Property, *Colloids Surf. A*, 2019, **578**, 123623. https://doi.org/10.1016/j.colsurfa.2019.123623

39. C. Huang, C. Hao, W. Zheng, S. Zhou, L. Yang, X. Wang, C. Jiang, and L. Zhu, Synthesis of Polyaniline/Nickel Oxide/Sulfonated Graphene Ternary Composite for All-Solid-State Asymmetric Supercapacitor, *Appl. Surf. Sci.*, 2019, **505**, 144589. https://doi.org/10.1016/j.apsusc.2019.144589

40. H. Vakili, B. Ramezanzadeh, and R. Amini, The Corrosion Performance and Adhesion Properties of the Epoxy Coating Applied on the Steel Substrates Treated by Cerium-Based Conversion Coatings, *Corros. Sci.*, 2015, **94**, p 466–475. https://doi.org/10.1016/j.corsci.2015.02.028

41. S.R. Nayak, K.N. Mohana, and M.B. Hegde, Anticorrosion Performance of 4- Fluoro Phenol Functionalized Graphene Oxide Nanocomposite Coating on Mild Steel, *J. Fluor. Chem.*, 2019, **228**, 109392. https://doi.org/10.1016/j.jfluchem.2019.109392

42. K. Qi, Y. Sun, H. Duan, and X. Guo, Corrosion-Protective Coating Based on a Solutionprocessable Polymer-Grafted Graphene Oxide Nanocomposite, *Corros. Sci.*, 2015, **98**, p 500–506. https://doi.org/10.1016/j.corsci.2015.05.056

43. B. Ramezanzadeh, M.H.M. Moghadam, N. Shohani, and M. Mahda-vian, Effects of Highly Crystalline and Conductive Polyaniline/ Graphene Oxide Composites on the Corrosion Protection Performance of a Zinc-Rich Epoxy Coating, *Chem. Eng. J.*, 2017, **320**, p 363–375. https://doi.org/10.1016/j.cej.2017.03.061

44. G. Christopher, M.A. Kulandainathan, and G. Harichandran, Comparative Study of Effect of Corrosion on Mild Steel with Waterborne Polyurethane Dispersion Containing Graphene Oxide Versus Carbon Black Nanocomposites, *Prog. Org. Coat.*, 2015, **89**, p 199–211. https://doi.org/10.1016/j.porgcoat.2015.09.022